

## PRECIPITATE EVOLUTION IN Zry-4 OXIDATION

P.B.Bozzano<sup>1</sup>, M. Ipohorski, R.A.Versaci

Departamento de Materiales - Unidad de Energía Nuclear,  
Comisión Nacional de Energía Atómica, Buenos Aires, Argentina.  
<sup>1</sup> Av. Gral. Paz 1499 (B1650KNA) San Martín, Buenos Aires, Argentina  
Tel: 54-11-6772-7282, Fax: 54-11- 6772-7632. [pbozzano@cnea.gov.ar](mailto:pbozzano@cnea.gov.ar)

### Abstract

The microstructure of Zr alloys has been a subject of study during the last decades due to its influence on the manufacturing of fuel elements sheaths for power reactors. In particular, Zircaloy – 4 is widely used as fuel cladding material.

It is known that during the initial oxidation of zirconium alloys thin coherent oxide films of ZrO<sub>2</sub> form over the whole surface, including the intermetallic particles lying on the surface. The precipitates are accommodated in the oxide film in a non- oxidized state, and then the zirconium present inside the precipitates is gradually oxidized to either cubic or tetragonal ZrO<sub>2</sub>. The precipitates into the oxide layer are subjected to a delayed oxidation as compared to the matrix, accompanied by the rejection of a significant proportion of their iron content. Previous works showed that precipitates undergo chemical composition changes after open furnace oxidation and it was suggested that a progressive Fe rejection towards the oxidized precipitate / oxidized matrix frontier takes place.

### Resumen

La microestructura de las aleaciones de circonio y en particular la microestructura del Zry-4, ha sido tema de estudio durante las últimas décadas debido a su empleo en la fabricación de vainas para elementos combustibles en reactores de potencia.

Es un resultado conocido que al iniciarse el proceso de oxidación, una delgada y coherente capa de óxido crece sobre toda la superficie. El proceso de oxidación de los precipitados es un tema más complejo: éstos son incorporados a la capa de óxido en estado metálico y que su proceso de oxidación comienza cuando están completamente rodeados de óxido. Este proceso trae aparejado un cambio en la microestructura de los precipitados (se oxida el Zr dentro de ellos y transforma a estructura cúbica o tetragonal) y un cambio en la composición química de los mismos: se produce una reyección de hierro hacia la interfase óxido - precipitado oxidado.

### 1. Introduction

Due to low neutron - capture cross - section, high mechanical strength, high thermal conductivity and good corrosion resistance in water and steam, Zircaloy – 4 (%wt Sn 1.45 - 1.5, Fe 0.18 - 0.24, Cr 0.07 - 0.13, O 1400ppm, Zr to balance) is widely used as fuel cladding material in nuclear reactors. Of all the alloying elements only Tin is in solid solution, and hence relatively uniformly distributed. Iron and chromium are essentially

insoluble in Zr at low temperatures (< 600° C) and they are, therefore, present almost entirely in the form of second phase particles [1]. There is only one intermetallic compound, Zr (Cr, Fe)<sub>2</sub>, which occurs in two structural forms, hexagonal (C14) and cubic (C15) [2,3]. The proportions of cubic and hexagonal Zr(Cr, Fe)<sub>2</sub> present in the sample, depends on the different fabrication routes. Both types of precipitates are

commonly present, usually with the hexagonal variant predominant. These intermetallic precipitates are about 10–1000 nm in diameter, depending on the fabrication conditions. The structure, composition, average size and morphology of the second phase precipitates are closely related to the corrosion behaviour of Zry-4 [4, 5, 6].

On the other hand, many studies were conducted in order to evaluate the oxidation process of Zirconium alloys in autoclave environments and in air. The air oxidation of Zry-4 cladding has been an interesting topic, but there exist relatively small amount of experimental data. The oxidation kinetics is generally divided in two main regions separated by a transition. During the first one, called the pre - transition region, the oxide formed is dense and composed by monoclinic and tetragonal  $ZrO_2$  crystallites, and the growth rate is cubic or quadratic. After the transition, the oxidation rate increases and then remains approximately constant in the second stage [7, 8]. Most of the outer part of the oxide layer is now porous and composed exclusively of monoclinic  $ZrO_2$  crystallites [9]. The tetragonal to monoclinic transformation has long been thought to play an important role in the oxidation kinetics transition. Tetragonal zirconia ( $ZrO_2$ ) is stable at temperatures above 1150°C, but can be stabilized at low temperatures in presence of high compressive stresses or by the introduction of elements into the zirconia lattice. Several hypotheses were proposed to explain this stabilization: effect of grain size, point defects configuration, presence of compressive stresses [10].

Less studies have been published on the mechanisms of precipitate incorporation into the oxide layer [11, 12, 13, 14]. It is known that during the initial oxidation of zirconium alloys a thin coherent oxide film of  $ZrO_2$  forms over the whole surface, including the intermetallic particles lying on the surface. The precipitates are accommodated in the oxide film in an non oxidised state [15], and then the zirconium present in the  $Zr(Cr, Fe)_2$  phase is gradually oxidised to cubic or tetragonal  $ZrO_2$ .

The precipitates in the oxide layer are subjected to a delayed oxidation as compared to the matrix, accompanied by the rejection of a significant proportion of their iron content at the precipitate / oxidised matrix interface [11]. Oxidation of iron and chromium can only occur at some point between the oxide / metal and the oxide / environment interfaces at which the effective oxygen partial pressure for these elements is reached. The formation of cubic  $ZrO_2$  in the precipitate is due to the high iron content which stabilises the cubic phase.

An empirical model has been proposed for the oxidation of the Laves phase  $Zr(Cr_{0.4}Fe_{0.6})_2$  (the most frequently observed in Zry-4 precipitates) [16]: at the beginning of the oxidation process at 650 °C, Zr transforms to  $Zr_xO_{2-x}$ . The other elements, Cr and Fe remain in metallic state until the O amount within the system increases to a value high enough to allow the oxidation of Cr. The oxidized Cr diffuses first into the  $Zr_xO_{2-x}$  and then migrates to the surface. As oxidation proceeds, the O partial pressure increases up to a value high enough for the Fe contained in  $Zr(Cr, Fe)_2$  to diffuse to the surrounding  $Zr_xO_{2-x}$ . Determinations showed a higher concentration of Cr on the external oxide surface “( $Zr_xO_{2-x}, Cr_yO_{2-y}$ )”, and evidence that Fe atoms migrate to an inner region than that of the oxidized – non oxidized frontier.

## 2. Experimental procedure

The material used for this work was commercial Zircaloy-4 as received furnished by Teledyne Wah Chang.

Samples in the form of 1.5mm thickness sheets were oxidised in an open furnace at 650 °C for different times, ranging from 1 to and 116 hours (See table I). The specimens were weighted before and after the oxidation process in order to obtain the weight gain, and therefore the oxidation kinetics.

After oxidation, the inner surface of the sheet was mechanically polished by hand grinding, and 3 mm

diameter disc specimens were ultrasonically cut. The discs were electropolished in order to remove any remaining base material (metal). The remaining oxide layer was then dimpled. The last thinning step of the oxide film was performed in an ion mill in order to control the thickness of the thin oxide film to be analysed.

Observations were carried out in a Phillips CM200 transmission electron microscope with an Energy Dispersive X-ray Spectrometer EDAX DX-4. The measured parameter was the Fe / Cr ratio within the precipitates.

### 3. Experimental results and discussion

#### 3.1 Reference Zircaloy-4

The microstructure and morphology of the precipitates present in Zry-4 have already been extensively studied by other authors [17, 18]. In the present work, for comparison, the reference material was first characterized: C14 hcp and C15 fcc Laves phases were observed in the electron micrographs, although relative quantities were not determined. Particles with diameters between 200 and 800 nm were the most frequently observed. Figure 1(a) shows a Zry-4 recrystallised micrograph and (b) typical bright-field image of a

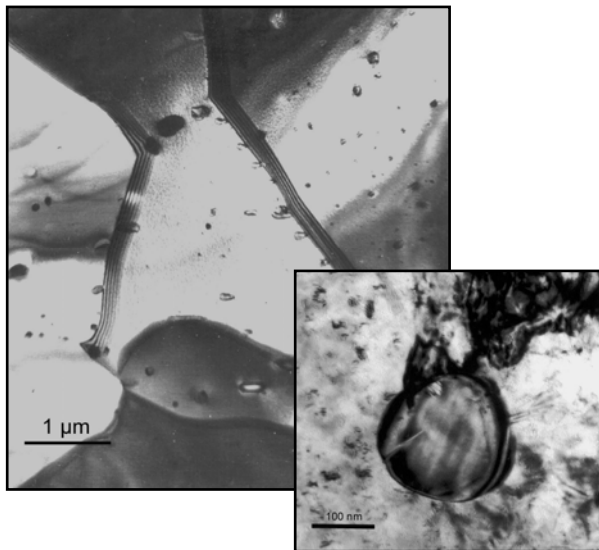


Fig. 1 (a) Zry-4 recrystallised and (b) bright-field image of a precipitate.

precipitate. The Fe / Cr ratio was also obtained, being the average value for the Cr / Fe ratio within the precipitates  $\approx 1.50$ . Figure 2 shows a typical EDS spectrum.

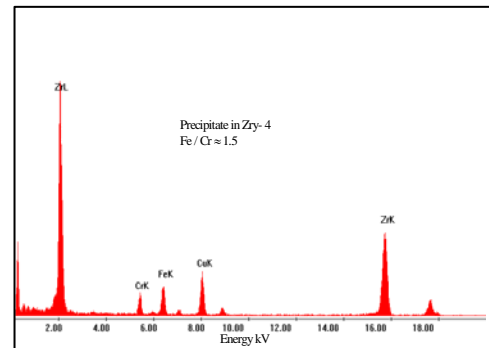


Fig. 2. EDS spectrum of a Zry-4 precipitate

#### 3.2 Oxidation Kinetics

Oxidation kinetics obtained on reference Zry-4 in open furnace (air) at 650°C, is presented in Figure 3. Table 1 shows details of the specimens. The oxidation kinetic curve, namely weight gain ( $dp$ ,  $mg/cm^2$ ) vs. reaction time ( $t$ , h), is in accordance with other authors [19]: our curve describes two main regions separated by a transition, like the oxidation in oxygen and steam. The first region is approximately quadratic and the second is linear with time.

Following Suzuki and Kawasaki procedure [8], the weight gain can be expressed as a function of time in the following way [20]:

In the pre- transition region:

$$dp^n = C_1 t \quad (1)$$

and in the post- transition region:

$$(dp - A)^n = C_2 (t - B) \quad (2)$$

where  $n$  is the reaction rate component,  $C_1$  and  $C_2$  are reaction rate constants ( $mg^n/h$ ),  $t$  is the reaction time ( $h$ ) and  $A$  and  $B$  are constants determined by fitting eq. (2).

Since it is very complicated to obtain strict values of  $A$  and  $B$ , in the present study we assumed that, as a

reasonable approximation,  $A$  can be well represented by the weight gain at the transition point ( $dp_t$ ) and  $B$  by the transition time ( $t_t$ ).

Hence eq. (2) is modified into the form

$$(dp - dp_t)^n = C_2(t - t_t) \quad (3)$$

Table 2 summarizes the values of  $n$  and  $C$  calculated by eq. (2) y (3), and lists an approximate rate constant  $C'$  determined by the following equation assuming that  $n=1$ , i.e.

$$C' = \frac{dp_e - dp_t}{t_e - t_t} \quad (4)$$

where  $dp_e$  is the weight gain at the last measurement and  $t_e$  is the reaction time for measuring  $dp_e$ .

Table 2 shows that the pre- transition yields  $n= 1.400$ , corresponding to mean a small deviation from a quadratic rate law. In the post- transition region the value of  $n= 1.004$  indicates a linear rate law.

Figure 4 shows an Arrhenius plot of the rate constant  $C'$  obtained in this work, together with data of [8]. This value of  $C'$  corresponding to 650°C (923 K), and those obtained by Suzuki and Kawasaki for lower oxidation temperatures, fit into a straight line when plotted against the reciprocal of the temperature  $T$ . The resulting Arrhenius plot could be described by the following equation, where  $R= 8.314$  J/ mol K and  $T$  the absolute temperature

$$C' = 2.16 \cdot 10^5 \exp\left(\frac{-1.23 \cdot 10^5}{RT}\right) \text{ mg/h} \quad (5)$$

Table I. Values of weight gain (mg) and time (h) of Zry-4 oxidized in open furnace (air) at 650° C

Time (h)	1	2	3	4	6	8	10	16	24	48	68	72	75	92	98	116
Weight gain (mg/cm <sup>2</sup> )	1.7	2.3	3.3	4.4	5.2	7.9	8	14.9	23.9	51.5	79.6	78.5	83.9	96.8	103.1	133.9

Table II. Rate constant and reaction time

Pre- transition region		Transition point			Post- transition region		Final state			
Range of time (h)	$n$	$C_1$ (mg <sup>n</sup> /h)	$p_t$ (mg/ cm <sup>2</sup> )	$t_t$ (h)	Range of time (h)	$n$	$C_2$ ( mg <sup>n</sup> /h)	$C'$ ( mg/h)	$p_e$ (mg/cm <sup>2</sup> )	$t_e$ (h)
1 a 10	1.40	1.85	8	10	10 a 116	1.002	1.16	0.84	134	116

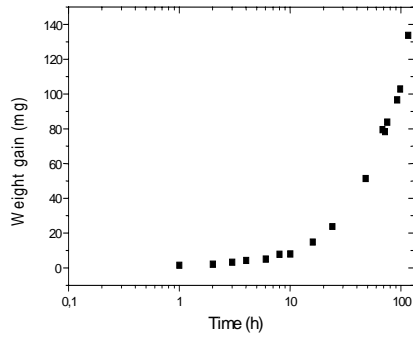


Fig. 3. Weight gain (mg) vs. time (h) of Zry-4 oxidized in open furnace (air) at 650° C.

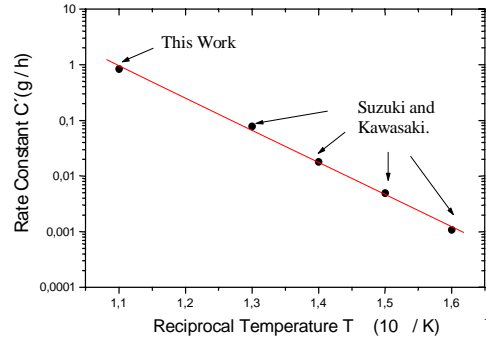


Fig. 4. Comparison of oxidation rate of Zry -4 in the post- transition region.

### 3.3 Microstructure of the oxide

The microstructure of the oxide was characterized by AEM. All the analyzed samples were selected from positions on the oxidation curve after the kinetic transition, corresponding to points where the post-transition porosity is developing in the oxide. Our observations showed that the oxide layer is now porous

and composed exclusively of monoclinic ZrO<sub>2</sub> crystallites of 10 – 50 nm. EDS analysis was also carried out and the typical composition of ZrO<sub>2</sub>, (Zr 33%, O 67%) was found (Figure 5).

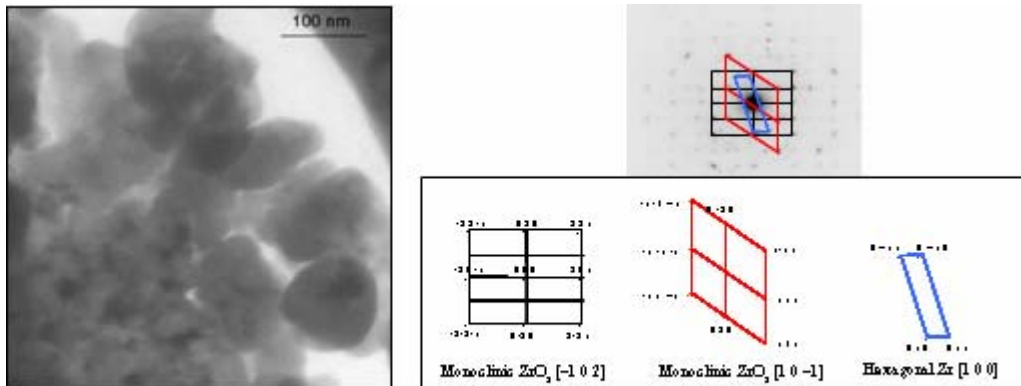


Fig. 5(a) Bright- field of oxidized Zry- 4.crystals, (b) (c) SAD pattern with indexed spots

### 3.4 Oxidation of Zr(Cr, Fe)<sub>2</sub> precipitates

All the analysed samples were selected from positions on the oxidation curves at the kinetic transition, corresponding to points where the post- transition porosity is being developed in the oxide.

Inside the oxide layer both non oxidized precipitates (i.e. original intermetallic precipitates) with a nominal Fe / Cr ratio of 1.5 (Figure 6) and oxidised precipitates with an Fe / Cr ratio decreased to 0.5 (Figure 7) were found.

The SAD pattern of the oxide crystallites close to an oxidised precipitate evidences the presence of cubic and monoclinic structure (Figure 8) The formation of cubic ZrO<sub>2</sub> in the adjacent matrix of the precipitate is due to the high iron content which stabilises the cubic phase.

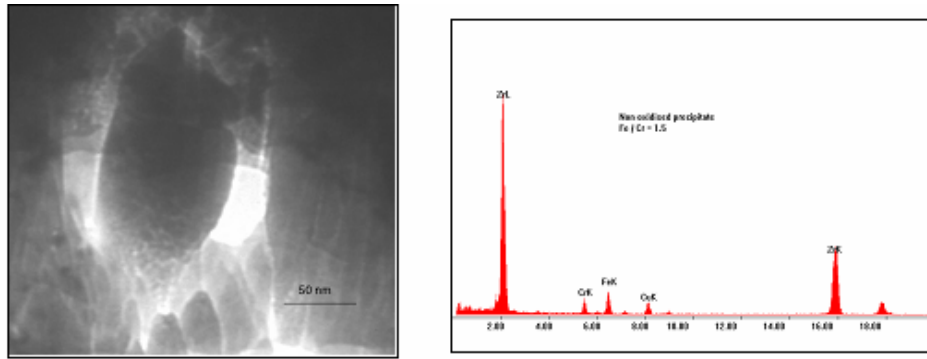


Fig. 6. a) Bright- field TEM image of an oxidized precipitate in fully oxidized Zry- 4 and (b)EDS spectrum with Fe / Cr ~ 0.5

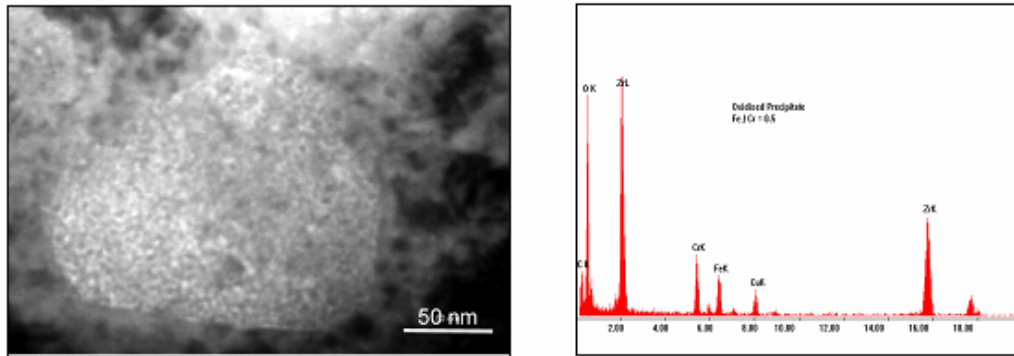


Fig. 7. a) Bright- field TEM image of an oxidized precipitate in fully oxidized Zry- 4 and (b) EDS spectrum with Fe / Cr ~ 0.5.

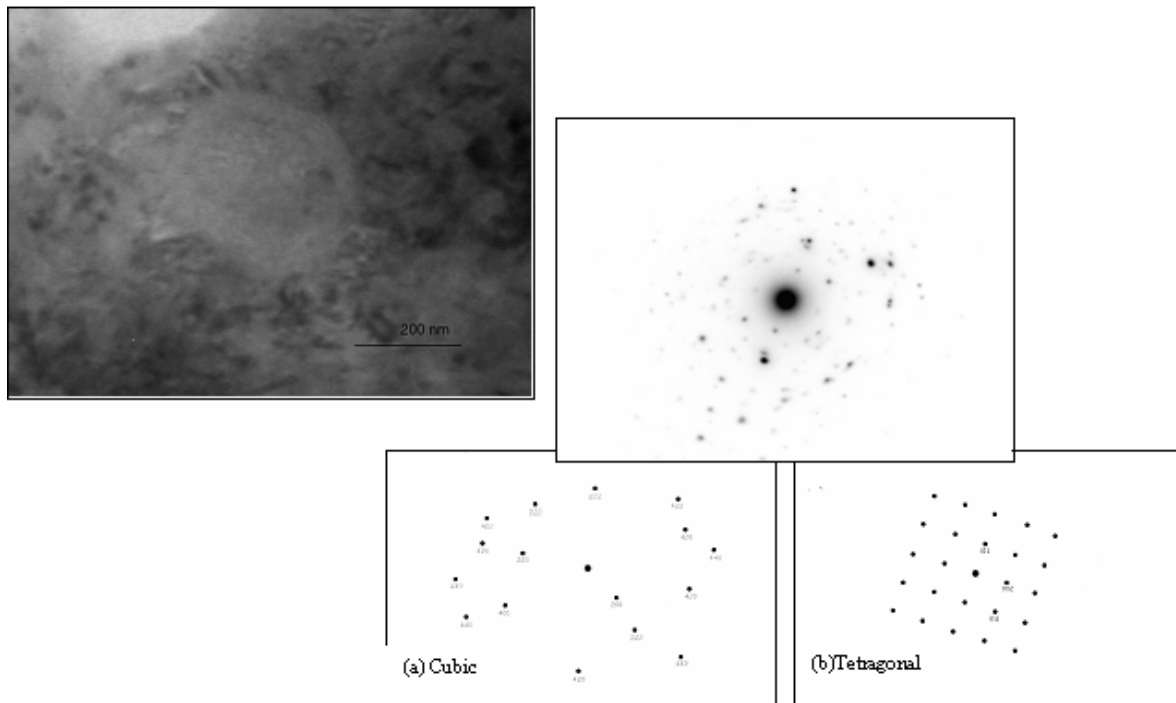


Fig. 8. SAD pattern of the oxide crystallites close to an oxidized precipitate. Spots evidence the presence of (a) cubic and (b) monoclinic structure

## CONCLUSIONS

- The above mentioned results show that the evolution of the precipitates, while incorporated into the Zircaloy oxide layer, is a rather complex process.
- It was observed that the zirconium matrix oxidises first, forming mostly monoclinic zirconia, while the  $Zr(Cr, Fe)_2$  precipitates remain non oxidised. The general trend observed is that  $Zr(Cr, Fe)_2$  precipitates are incorporated in a non oxidised state into the oxide layer and became oxidised later.
- The mean size of the crystallites formed in the precipitates is also different from those formed in the matrix: the former are smaller and spherically shaped.

- The adjacent matrix of the oxidised precipitate was identified as cubic / tetragonal  $ZrO_2$ . Therefore it is possible that the alloying elements present in the oxidised precipitates contribute to the stabilisation of the tetragonal / cubic phase.
- The  $Zr (Cr_{0.4}Fe_{0.6})_2$  Laves phases undergo a selective oxidation process: a part of the original C14Laves phases remains; however, also  $Zr_x O_{2-x}$ ,  $Cr_2O_3$ ,  $\alpha-Fe$  and  $(Fe, Cr)_x O_y$  structures were found.
- Mössbauer Spectroscopy can be used to distinguish in detail the different stages of the oxidation process, in particular the evolution of the iron bearing phases [12].

## REFERENCES

1. D.Charquet, R.Hahn, E.Ortlieb, J.P.Gros and J.F.Wadier, Proc. 8<sup>th</sup> Int.Symp. on Zirconium in the Nuclear Industry, ASTM- STP 1023, Philadelphia 1988 p.405.
2. R.A.Versaci and M.Ipohorski, J.Nucl. Mater. 80(1979)180, *ibid.* 116(1983)321.
3. X.Y.Meng and D.O.Northwood, J.Nucl. Mater. 137(1986)217.
4. P.Rudling, K.L.Vannsesjö, G.Vesterlund and A.R.Massih, Proc. 7<sup>th</sup> Int.Symp. on Zirconium in the Nuclear Industry, ASTM- STP 939, Philadelphia 1987 p.292.
5. H.G.Weidinger, H.Ruhmann, G.Cheliotis, M.Maguire and T.L.Yau, Proc. 9<sup>th</sup> Int.Symp. on Zirconium in the Nuclear Industry, ASTM- STP 1132, Philadelphia 1991 p.
6. D.G.Franklin and P.M.Lang, Proc. 9<sup>th</sup> Int.Symp. on Zirconium in the Nuclear Industry, ASTM- STP 1132, Philadelphia 1991 p.3.
7. B.Cox, J.Nucl. Mater. 29(1969)50.
8. M.Suzuki and S.Kawasaki, J.Nucl. Mater.140(1986)32.
9. F.Garzarolli, H.Seidel, R.Tricot and P.Gross, Proc. 9<sup>th</sup> Int.Symp. on Zirconium in the Nuclear Industry, ASTM- STP 1132, Philadelphia 1991 p. 416.
10. Godlewski , Proc. 10<sup>th</sup> Int.Symp. on Zirconium in the Nuclear Industry, ASTM- STP 1245, Philadelphia 1994 p. 663.
11. T.Kubo and M.Uno, Proc. 9<sup>th</sup> Int.Symp. on Zirconium in the Nuclear Industry, ASTM- STP 1132, Philadelphia 1991 p. 476.
12. P.B.Bozzano, C.Ramos, F.Saporiti, P.A.Vazquez, R.A.Versaci, C.Saragovi, J.Nucl. Mater. 328(2004)225.
13. D.Pêcheur, F.Lefebvre, A.Motta, C.Lemaignan and D.Charquet, Proc. 10<sup>th</sup> Int.Symp. on Zirconium in the Nuclear Industry, ASTM- STP 1245, Philadelphia 1994 p. 687.
14. X.Iltis, F.Lefebvre and C.Lemaignan, J.Nucl. Mater. 224(1995)121.
15. R.A.Versaci, P.B.Bozzano and M.Ipohorski. Proc. of the EUROMAT 96, Conference on Materials and Nuclear Power, 21- 23 October 1996, Bournemouth, United Kingdom.p.411.

Bozzano, *et al.*

16. P.B.Bozzano., M.Ipohorski and R.A. Versaci, Proc. Electron Microscopy Symposium ICEM 14 (1998)105.
17. J.A.Sawicki, J.Nucl. Mater. 228(1996)238.

Acta Microscópica, Vol. 13., Nos. 1 y 2, 2004, pp. 47–54

18. W.Xiao and C.Ma, J.Nucl. Mater. 255(1998)67.
19. J.Nakamura, M.Hashimoto, T.Omoto and S.Kawasaki, J.Nucl. Mater. 200(1993)256.
20. B.Cox, J.Nucl.Mat. 336(2005)331.